

# Barrier potential for laser written graphitic wires in diamond

I. Haughton<sup>1</sup>, I. Lopez Paz<sup>1</sup>, M. McGowan<sup>2</sup>,  
A. Oh<sup>1\*</sup>, A. Porter<sup>1</sup>, P. S. Salter<sup>3</sup>, O. Allegre<sup>1</sup>

1. School of Physics and Astronomy, University of Manchester, UK

2. School of Electrical and Electronic Engineering, University of Manchester, UK

3. Department of Engineering Science, University of Oxford, UK

November 6, 2020

## Abstract

Diamond substrates supporting an internal array of conductive graphitic wires inscribed by a femtosecond pulse laser, are useful for the detection of ionising radiation in a range of applications. Various parameters involved in the laser fabrication process were investigated in this paper to understand their impact on the electrical properties of the wires. The study revealed an effect, whereby the wires exhibit insulating behaviour until a barrier potential is overcome. When high enough voltages are applied, the wires display ohmic behaviour. The magnitude of the barrier potential, which in some cases exceeds 300 V, is shown to be strongly dependent on the laser fabrication parameters. Through process optimisation, the potential barrier may be minimised and effectively removed, coinciding with reduced values of the wire resistance.

the diamond using a femtosecond pulse laser [9]. The 3D geometry of the electrodes significantly increases the radiation tolerance of the detector with respect to the ‘planar’ geometry [10]. Such improvement is a consequence of decoupling the inter-electrode distance from the detector thickness. Thus, for the same particle traversing the detector in either geometry, the same amount of charge carriers is generated. However, as the charge collection distance may be shorter in the 3D design, the probability of the charges being trapped in intermediate energy levels in the diamond is reduced. While the charge collection properties and radiation resistance of such detectors has previously been investigated [11, 7, 8, 12], understanding the electrical properties of the graphite wire electrodes and their effect on overall performance is still to be fully explored. In this paper we investigate the electrode electrical properties as a function of various laser fabrication parameters.

## 1. INTRODUCTION

Synthetic diamonds produced by the chemical vapour deposition (CVD) process are used for the detection of ionising radiation in applications of dosimetry, beam monitoring and particle tracking. Conventional devices use metallic electrodes on the top and bottom surfaces of the diamond plates in a ‘planar’ detector configuration [1, 2, 3, 4]. In the last decade, so called ‘3D diamond detectors’ have been investigated [5, 6, 7, 8], which feature column-like graphitic electrodes written within the bulk of

## 2. METHOD

Diamond samples were inscribed with graphitic wires passing through the full thickness (thicknesses of 400 - 500  $\mu\text{m}$ ) using a regeneratively amplified Ti:Sapphire laser (Spectra-Physics Solstice) with wavelength  $\lambda = 790 \text{ nm}$ , a pulse repetition rate of 1 kHz and  $\approx 250 \text{ fs}$  pulse duration.

The samples used for these studies were produced by ElementSix and consisted of "optical grade" (less than 5ppm Nitrogen content) and "electronic grade" diamonds (less than 50ppb Nitrogen content) [13]. The samples were

\*Corresponding author: alexander.oh@manchester.ac.uk

an "optical grade" (100) oriented single-crystal CVD diamond of dimensions  $4 \times 4 \times 0.5 \text{ mm}^3$  (sCVD-0), an "electronic grade" single-crystal diamond (sCVD-1), and an "optical grade" poly-crystalline diamond (pCVD-1), both with nominal dimensions of  $4 \times 4 \times 0.4 \text{ mm}^3$  and  $5 \times 5 \times 0.5 \text{ mm}^3$ , respectively. No special surface preparation was applied prior to laser processing. Sample sCVD-0 was processed in 2017, and samples sCVD-1 and pCVD-1 were processed in 2019.

The laser power was controlled with a rotating half-waveplate in conjunction with a polariser. The beam from the laser was expanded and directed on to a liquid crystal phase-only spatial light modulator (SLM) (Hamamatsu X10468-02). A beam expansion of  $8\times$  ensured that the laser intensity was effectively uniform across the area of the SLM display. The SLM output was then imaged onto the pupil plane of a microscope objective with a high numerical aperture (NA=0.75) in "4f" configuration. The diamond sample was mounted on a precision 3D translation stage (Aerotech ABL10100 (x,y) and ANT 95V (z)) beneath the objective lens. A transmission optical microscope was used for spatial alignment using the same objective lens as the laser processing, allowing for high resolution imaging of the sample during processing. The fabrication process was initiated by focusing the laser on the rear surface of the diamond and drawing a graphitic seed through to the front surface by axial translation of the sample away from the objective lens (*1 pass*). In addition, we investigated whether the wire properties could be improved through overwriting, by repeating the identical fabrication procedure on the same wire multiple times (*multi-pass*).

When focusing the laser beam inside diamond for wire fabrication, the ability to achieve the required focal intensity for the given numerical aperture is hindered by optical aberrations. Refraction of light at the diamond surface causes a depth-dependent distortion of the laser focus and an associated reduction in the focal intensity [14]. We use adaptive optics aberration correction to remove distortion and restore diffraction limited performance [15]. The SLM in the laser beam path is programmed to introduce a phase change that can counteract the

aberration induced from refraction at the diamond surface. The aberration correction is continuously updated during the laser processing for different focal depths within the diamond, using feedback from the translation stages. As a control test, a set of graphitic wires were additionally processed without aberration correction, by maintaining a flat phase on the SLM throughout the fabrication.

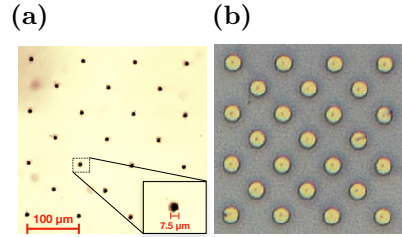


**Figure 1:** Optical microscope image of the diamond surface with an array of graphitic columnar wires before (a) and after (b) metallisation. The opposite surface has a blanket metallisation for better electrical contact with the probe station chuck during electrical characterisation.

After laser processing, a chromium-gold surface metallisation was applied by evaporation to the samples to provide an electrical contact to both sides of a graphitic column. Afterwards, the sample set sCVD-1 and pCVD-1 (sCVD-0) were annealed for 5 minutes at a temperature of  $400^\circ\text{C}$  ( $450^\circ\text{C}$ ) in a  $\text{N}_2$  atmosphere. One surface was blanket metallised to form a common base electrode, while the other was structured to create  $\approx 25 \mu\text{m}$  islands above each wire (see Fig 1). This enabled simple electrical characterisation of individual wires by mounting the sample in a probe station. The blanket metallisation on the bottom surface provides full electrical contact with the probe station chuck, while the individual islands on the top surface are contacted via probe needles. The current was measured as a function of applied DC voltage across a particular graphitic wire. The gradient of the current-vs-voltage plot (I-V curve) was taken as a measurement of the wire conductance (the reciprocal of the electrical resistance). Electrical measurements were repeated on several sample wires up to 25 times across different

sessions with results showing a low dispersion of measured values and no clear time dependence, affirming a high level of repeatability in the electrical characterisation.

### 3. RESULTS

A preliminary scan of the parameter space was performed on sample sCVD-0. The axial translation speed of the diamond relative to the fixed laser focus was varied between 5 - 30  $\mu\text{m/s}$ . A physical translation speed of the sample  $v$  in the axial direction in fact corresponds to a focal displacement speed  $nv$ , where  $n = 2.4$  is the refractive index of the diamond. The axial dimension of the laser focus can be estimated as  $\Delta z = 2n\lambda/\text{NA}^2 = 6.7\mu\text{m}$ , so that with a 1 kHz pulse repetition rate ( $f_p$ ), the effective number of pulses interacting with each part of the diamond during column fabrication is  $f_p * \Delta z/nv$ . Meanwhile the laser pulse energy was varied between 50 - 300 nJ, with different ranges used dependent on translation speed to ensure comparable cumulative fluence for the wires. The processing was also tested with linear and circular polarization states of the fabrication laser. To obtain reasonable statistics, each variable configuration was repeated to create at least 5 individual wires.

Example I-V characteristics for the fabricated wires are shown in Fig. 2. Several of the wires exhibited classic ohmic behaviour [16], as seen by the highly linear I-V relationship in the top plot. However, for many of the measured graphitic columns, we observed unexpected response with very high resistance at low voltages, such that the wires were initially considered as insulating. Nevertheless, applying higher voltages still, we found that linear ohmic behaviour resumed beyond some "barrier potential"  $|U_\phi|$  (see an example in Fig. 2, b).

The resistance and barrier potential values were obtained for individual wires by fitting the I-V curves with a first order polynomial in the ohmic regions. The reciprocal of the linear slope is the resistance  $R$  for each voltage polarity, while the point of intersection of the linear fit with the zero current value was used to define the barrier voltage region. The difference between the two intersection points was taken

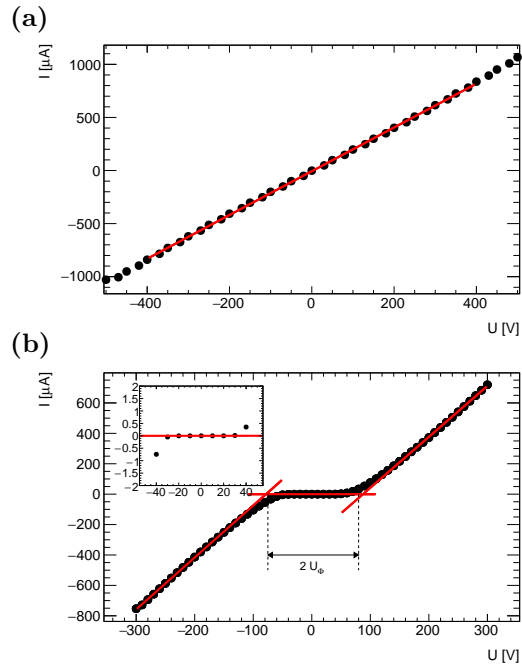


**Figure 2:** An example of the I-V characteristics of a wire displaying an ohmic behaviour (a) fabricated with 100nJ pulses at a speed of 10  $\mu\text{m/s}$  and a barrier potential effect (b) for a wire fabricated with the same pulse energy but at a speed of 45  $\mu\text{m/s}$ . Plot (b) shows in addition an inset plot of the central area with the same units as the main plot.

as a measurement of  $2|U_\phi|$ , as shown in Fig. 2.

The results for  $|U_\phi|$  and  $R$  are presented in Fig. 3 as a function of pulse energy for the fabrication laser. The distribution of resistance and barrier potential values for columns fabricated with the identical processing parameters was non-Gaussian, so we use the median of the distribution as the quoted value of the resistance and barrier potential. The 16% and 84% percentile points represent the uncertainty of the measurements, giving a 68% confidence level interval. The results show a steady decrease in both  $|U_\phi|$  and  $R$  with increasing laser pulse energy at axial translation speeds below 20  $\mu\text{m/s}$ , although it is noted that the observed barrier potential has values above 100 V for the majority of wires. The barrier potential is particularly high at larger translation speeds, exceeding 400 V for speeds of 30  $\mu\text{m/s}$ , which is potentially related to the reduced pulse dosage. The data

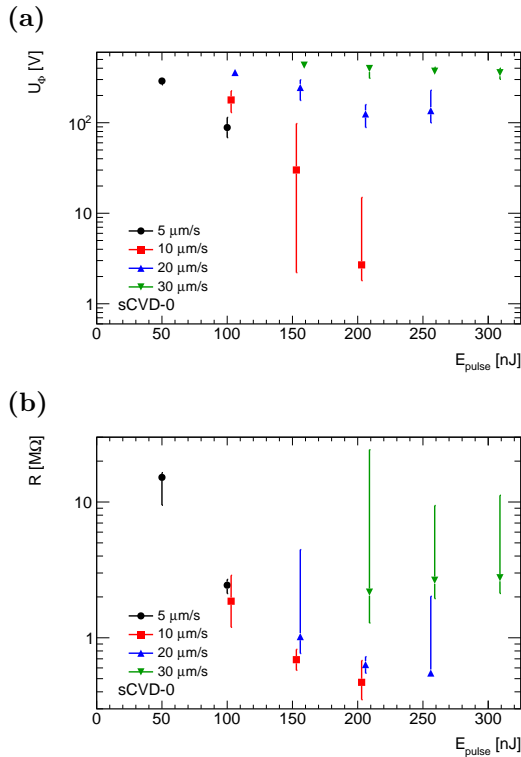


**Figure 3:** Measured values of the barrier potential  $|U_\phi|$  (a) and resistance (b) for sample sCVD-0 as a function of laser pulse energy.

from Fig. 3 additionally shows that the wires with the lowest barrier potential correlate with the wires displaying lowest values of resistance outside of the barrier potential window, holding promise for device fabrication.

The initial study revealed no clear dependence for the polarisation of the laser on either the resistance or barrier potential of the wires, with those fabricated with linear and circular displaying results within the given uncertainty ranges. However, there was a strong dependency for both  $|U_\phi|$  and  $R$  on the aberration correction used during laser fabrication. Wires processed with a static phase displayed on the SLM (no aberration correction) all exhibited  $|U_\phi| > 200$  V and  $R > 2$  MΩ, while wires fabricated at equivalent speed and pulse energy (10 μm/s and 200 nJ) with a dynamic phase on the SLM to fully correct aberration at each depth were characterised with  $|U_\phi| < 20$  V and  $R < 0.7$  MΩ.

Thus, it can be seen that maintaining focal quality of the fabrication laser through aberration correction is important in minimising both barrier potential and resistance for the wires. This may also explain in part the poor performance of wires fabricated at high axial translation speeds, since the response time of the SLM (approximately 30 Hz) is insufficient to fully correct the rapidly changing depth dependent aberration.

To investigate further, an additional two diamond samples were processed: a detector quality single-crystal diamond (sCVD-1) and an optical grade poly-crystalline diamond (pCVD-1). Drawing from the results of tests on sCVD-0, the light polarisation was set to linear and a fixed writing speed of 10 μm/s was used throughout. It was clear from the initial study that accurate focusing was important, so software improvements were made to the automated process for aberration correction while axially scanning during column fabrication. The laser fabrication was performed using a pulse energy range of 70 - 170 nJ. Results showing the dependence of the measured electrical resistance and barrier potential on the pulse energy is shown in Fig. 4 for samples sCVD-1 and pCVD-1.

The results in Fig. 4 for  $|U_\phi|$  and  $R$  in samples sCVD-1 and pCVD-1 display a similar trend to sCVD-0, with the barrier potential and resistance decreasing for higher pulse energy. However, the results for the barrier potential at comparable energies and speeds are reduced by two orders of magnitude for sCVD-1 and pCVD-1, to the point where it becomes almost negligible. This large reduction in barrier potential can possibly be explained by a higher level of optimisation in the aberration correction between the two processing runs, with improvements made in the calibration of the aberration settings. Before wire fabrication, the aberration correction was optimised at a series of depths inside the diamond to minimise the pulse energy required for fabrication. The optimisation was carried out for low order Zernike phase aberrations (up to primary spherical  $Z_{4,0}$ ) as well as the depth dependent spherical aberration [15]. In addition, improvements were made to the software to increase the update rate of the SLM following feedback from the translation stages. Nevertheless, further study is needed to fully discount



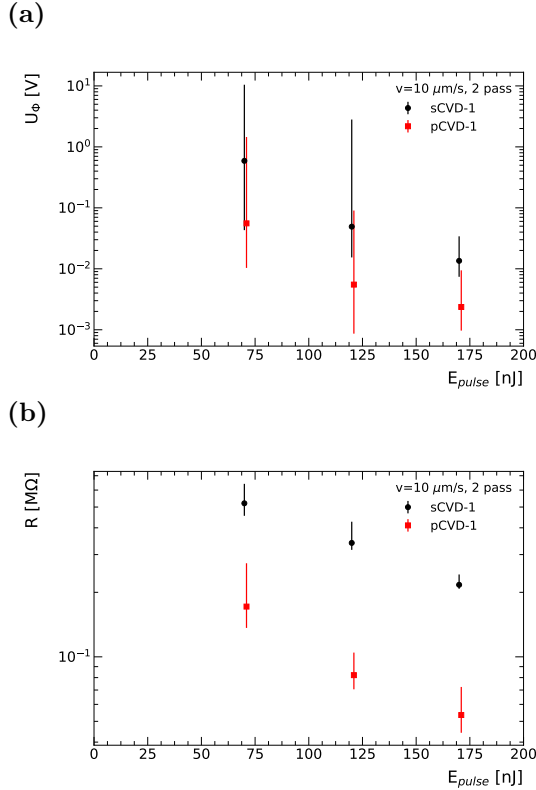


**Figure 4:** Values of barrier potential (a) and resistance (b) for samples sCVD-1 and pCVD-1 with a single writing speed ( $10 \mu\text{m/s}$ ) as a function of laser pulse energy. The markers represent the median value and the uncertainty bars indicate the 68% confidence level interval.

the potential for significant variation in wire performance between different processing runs.

All samples exhibited a similar trend where the measured resistance decreased for increasing beam energy. However, the fabricated electrodes are also seen to be of greater diameter for larger pulse energies. Fig. 5 shows the values of resistivity calculated for wires fabricated in sCVD-1 and pCVD-1 as a function of pulse energy, where we observe that the resistivity appears to be constant, within uncertainties, over this energy range. This indicates that increasing the beam pulse energy does not affect the overall graphite density of the column, but only enlarges its cross-section.

Fig. 6 shows relative differences of the resistance and barrier potential measured for

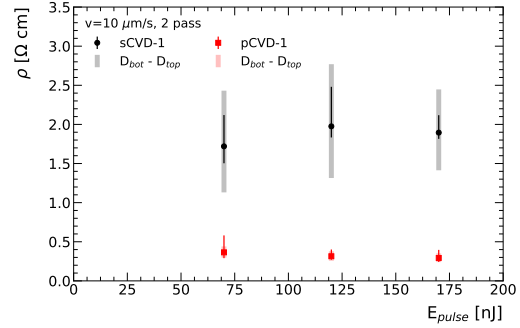


**Figure 5:** Calculated resistivity values of wires fabricated in samples sCVD-1 and pCVD-1 as a function of laser pulse energy with a single writing speed ( $10 \mu\text{m/s}$ ). The markers represent the median resistivity value calculated with the average of the diameters in both surface of the diamond, while the shaded area represents the variation of resistivity using the wire diameter on either side.

columns at positive and negative voltage polarity. The resistance measured in either polarity typically differ by less than 10%. The difference between barrier potentials typically tends to be larger, particularly in the single-crystal sample, where the positive barrier potential is on average 44% larger than the negative voltage polarity.

The spatial distribution of the observables (barrier potential, resistivity) did not exhibit any pattern that could be related to e.g. changing laser parameters over the processing time.

Overwriting of laser written graphitic tracks by multiple passes of the laser beam has previously been shown as effective in reducing resistivity of the wires [17, 18]. We investigated the effect in samples sCVD-1 and pCVD-1 by overwriting the graphitic columns and using a ‘double-sided’ fabrication procedure. For the double-sided process, two passes of the laser focus were performed over the full thickness of the diamond slab. Subsequently the sample was flipped and the wire was re-processed, this time starting from the top surface (wire seed side) to half the thickness and then back towards the top surface (see Fig. 7(b)). The aim of this process was to counter low levels of graphitisation on the seed side of the diamond, where the largest optical aberration is encountered (see Fig. 7(a)).

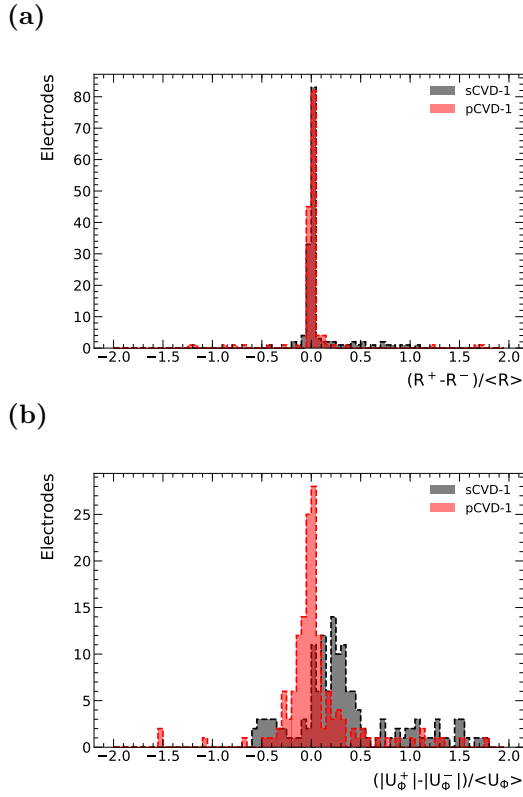


**Figure 6:** Histograms of the wire resistances (a) and barrier potentials (b) displaying asymmetry over relative potentials between wires fabricated in samples sCVD-1 and pCVD-1.

Due to the thickness of the diamond samples, the aberration at the seed surface is large, corresponding to an RMS phase of 7.4 radians across the objective pupil, and therefore difficult to fully compensate with the SLM.

The results for repeating the graphitisation process along the same column are shown in Fig. 8 for sCVD-1 and pCVD-1. There is a small reduction in the resistance of the wire for the sCVD-1 sample, with a further slight improvement for the ‘double-sided’ approach, from  $340^{+87}_{-24}$  k $\Omega$  to  $253^{+12}_{-9}$  k $\Omega$ . In addition, the resistance values have a significantly smaller spread across the 25 wires processed in the ‘double-sided’ scheme. However, the effect of overwriting seems non-existent on the measured resistance of wires in the polycrystalline pCVD-1 sample.

The graphitic wire diameter was additionally measured for the overwritten wires on samples

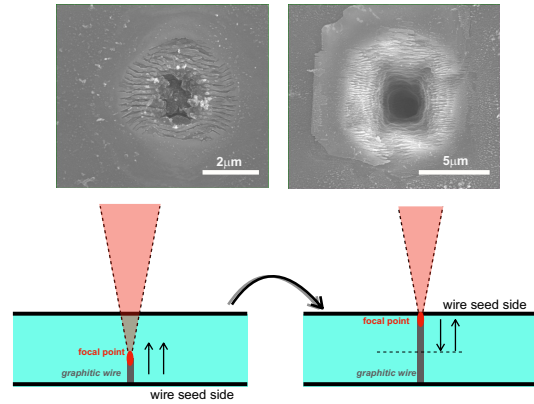


**Figure 7:** Top figure shows a SEM pictures of a column in sCVD-0 on the seed side (left) and opposite side (right) produced with a single sided process. The bottom figure is a sketch showing the double-sided processing process. The inscribing starts from the back surface of the diamond, passing through to the top. This is done twice to the wire (2 passes). Afterwards, the sample is flipped and the same wire is overwritten, this time starting from the top surface (wire seed side) to half the thickness and then back towards the top surface.

sCVD-1 and pCVD-1 by taking microscope images of the front and back surfaces of the diamond prior to metallisation. The measured diameters for the electrode arrays are shown in the lower plot of Fig. 8. There is notable difference in the electrode diameter on the opposite surfaces of the diamond, which is particularly pronounced when there is no aberration correction provided by the SLM. The dynamic use of the SLM has a significant impact on the measured values of the column diameters, with a marked increase on the seed surface. The small remaining disparity can be resolved with the double-sided procedure to create a comparable electrode diameter on both sides of the diamond, indicating a more uniform formation along the full length of the graphitic wire.

To further study the effect of adaptive optics, electrical characterisation was performed on the graphitic columns produced with and without aberration correction from the SLM in sCVD-1 and pCVD-1. The correlation of barrier potential with column resistance are shown in Fig. 9. All samples showed consistent behaviour:

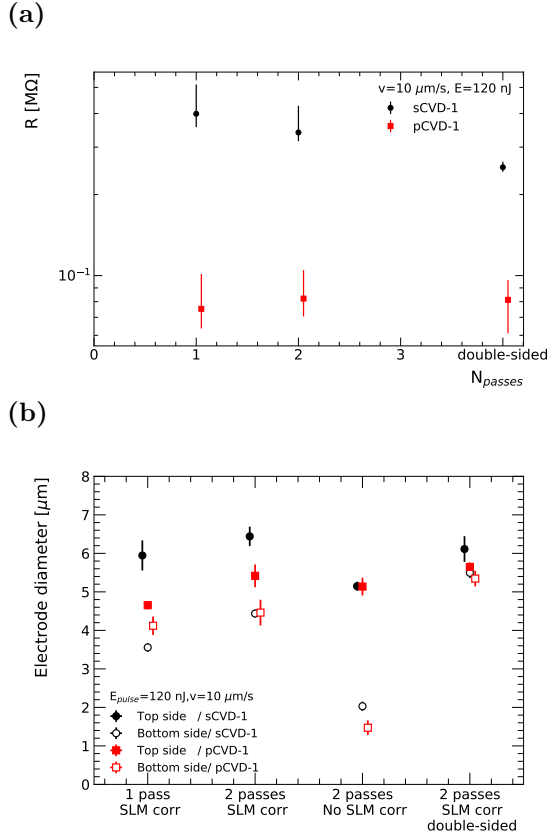


**Figure 8:** The plot (a) shows measured values of the electrical resistance for electrodes fabricated in sCVD-1 and pCVD-1 as a function of number of laser passes along each column. A fixed pulse energy (120 nJ) and writing speed ( $10 \mu\text{m/s}$ ) was used throughout. Average diameters of the associated columns are shown in plot (b). 'Bottom side' refers to the size of the wire at the seed surface of the diamond, i.e. where graphitisation of columns were started. Data points are slightly offset along the horizontal axis purely to aid visibility.

those processed using adaptive optics exhibit a significantly lower resistance compared to the samples processed without optical corrections. The observed barrier potentials are negligible when utilising the adaptive optical aberration correction, while being  $\sim 100 \text{ V}$  when maintaining a flat phase on the SLM and otherwise the same processing parameters. In conjunction with the results of the electrode diameter in Fig. 8, this demonstrates the effectiveness of the SLM correction to maintain a consistent focal spot size throughout the full depth of the diamond. Without adaptive optics corrections, the focal spot is significantly distorted by aberrations resulting in a smaller electrode diameter at the seed surface and wires with much inferior electrical properties.

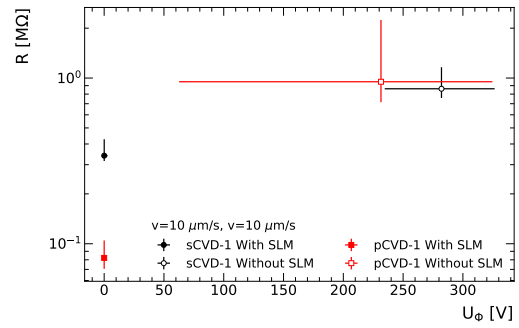


**Figure 9:** Correlation between barrier potential and resistance for columns produced with and without dynamic optics corrections in samples sCVD-1 and pCVD-1.

## 4. DISCUSSION

To our knowledge, this is the first observation of a barrier potential for laser written graphitic wires inside the bulk of diamond. One possible explanation is that microscopic gaps exist within the graphitic network of the wire, and that charge transport can only be achieved by surpassing the breakdown voltage of these structures, which is then equal to the observed barrier potential. Previous experiments exploring the microscopic structure of the laser written wires via scanning and transmission electron microscopy have shown multiple intersecting planes of graphitic sheets with a thickness of

40-100 nm [19, 20]. It was found that only  $\approx 4\%$  of the wire cross-sectional area contained conductive  $sp^2$  bonded carbon, while the remainder was unmodified diamond. It is expected that the graphitic sheets need to form a linked network in order to establish a conductive wire on the macroscopic scale. The low density of graphite in the wires would enhance the probability that the conductive path might be interrupted, giving rise to the barrier potential observed here. The higher barrier potentials observed for columns produced without aberration correction correlates with prior observations of lower graphite conversion in these conditions [17], making micro-gaps in the conductive path more probable. The overall low proportion of  $sp^2$  bonded carbon within the wire cross-section [21] can also help explain why the resistivity values reported for such wires are significantly higher than that for poly-crystalline graphite.

An interesting effect was observed in experiment that the polycrystalline diamond samples emitted blue light when applying voltages above  $\sim 200$  V to graphitic wires with significant barrier potentials. Such electroluminescence can possibly be explained by a conduction mechanism across micro-gaps that relies upon breakdown of the electric field, and associated injection of carriers into the diamond, which may subsequently become trapped at electronic states within the band-gap. This effect has been observed previously in pCVD diamond samples [22] and between closely spaced graphitic electrodes in pCVD diamond [23].

Despite the fact the pCVD-1 sample ( $500\text{ }\mu\text{m}$ ) is thicker than the sCVD-1 sample ( $400\text{ }\mu\text{m}$ ), columns produced under similar conditions showed systematically lower resistances in the polycrystalline material. The wires produced on sCVD-1 tend to show a larger diameter on the top surface (opposite to the writing seed side) compared to sample pCVD-1. This could indicate an intrinsic difference in the graphitisation process between single- and poly-crystal diamond that could be related to internal stress (more pronounced in poly-crystalline material) or crystal orientation. A similar trend in electrode diameter was observed in a previous study [24] using a similar experimental set-up,

although the larger laser pulse energy uncertainties prevented a conclusive result. Nevertheless, the results are promising for the fabrication of electrical devices inside cheaper polycrystalline material.

## 5. CONCLUSION

The impact of the laser fabrication parameters on the properties of graphitic wires produced inside both synthetic single-crystal and poly-crystalline CVD diamond samples has been studied. Wires fully passing through the CVD samples were fabricated at different laser beam energies, processing speeds and light polarisation. The column quality was assessed by measurements of electrical resistance and diameter. For many of the measured columns a barrier potential effect was observed, where the current is negligible through the column until the applied voltage is greater than the barrier,  $|U_{bias}| > |U_\phi|$ , after which the column shows ohmic behaviour.

Higher laser pulse energy during fabrication creates graphitic wires with larger diameter and lower resistances and barrier potentials. After calculating the resistivities of the columns in the finer parameter scan, no dependence is observed, within uncertainties, with the pulse energy ( $70 - 170$  nJ,  $10\text{ }\mu\text{m/s}$ ). This indicates that the beam pulse energy does not affect the graphite density of the columns. Columns that are written slower and with more repetitions show the lowest resistance and barrier potentials. Light polarisation of the fabrication laser was not observed to have a significant effect on the wire properties within experimental uncertainties. The effect of adaptive optical aberration correction during fabrication was studied and found to be a key factor determining the quality of the graphitic wires. Through the use of accurately calibrated aberration correction, the barrier potential can be made negligible, coinciding with minimum values of wire resistance. The same trends were observed in three different samples in two different parameter space scans. The resistances and barrier potential measurements were shown to be reproducible over multiple measurements.

The experimental findings of the barrier potential in this study can hopefully provide additional useful information in understanding

the charge transfer properties of laser written graphitic wires in diamond. Evaluation of the barrier potential will be an important factor when characterising new schemes for laser processing wires, such as the use of Bessel beams [25, 26]. The barrier potential is also a highly relevant consideration as more complicated device architectures utilising laser written wires in diamond start to emerge, with designs comprising wire junctions [27] and intentional gaps in the conductive network [28].

### ACKNOWLEDGEMENTS

The authors would like to thank Dmitry Hits from ETH Zürich for the surface metallisation of the sCVD-1 and pCVD-1 samples.

AO would like to acknowledge support from STFC grants ST/M003965/1/, ST/P002846/1. PSS gratefully acknowledges financial support from EPSRC UK, grant number EP/R004803/01.

The work was performed in the framework of the CERN-RD42 collaboration.

### REFERENCES

- [1] A. J. Edwards, B. Brau, M. Bruinsma, P. Burchat, H. Kagan, R. Kass, D. Kirkby, B. A. Petersen, and M. Zoeller, “Radiation monitoring with diamond sensors in babar,” *IEEE Transactions on Nuclear Science*, vol. 51, pp. 1808–1811, Aug 2004.
- [2] R. Eusebi, R. Wallny, R. Tesarek, P. Dong, A. Sfyrila, W. Trischuk, and C. Schrupp, “A diamond-based beam condition monitor for the cdf experiment,” *2006 IEEE Nuclear Science Symposium Conference Record*, vol. 2, pp. 709–712, Oct 2006.
- [3] V. Cindro, D. Dobos, I. Dolenc, H. Fraiskölbl, A. Gorišek, E. Griesmayer, H. Kagan, G. Kramberger, B. Macek, I. Mandić, M. Mikuž, M. Niegl, H. Pernegger, D. Tardif, W. Trischuk, P. Weilhammer, and M. Zavrtanik, “The ATLAS beam conditions monitor,” *Journal of Instrumentation*, vol. 3, pp. P02004–P02004, feb 2008.
- [4] G. Antchev, P. Aspell, I. Atanassov, V. Avati, J. Baechler, V. Berardi, M. Berretti, E. Bossini, U. Bottigli, M. Bozzo, P. Broulím, A. Buzzo, F. Cafagna, M. Catanesi, M. Csanád, T. Csörgő, M. Deile, F. D. Leonardis, A. D’Orazio, M. Doubek, K. Eggert, V. Eremin, F. Ferro, A. Fiergolski, F. Garcia, V. Georgiev, S. Giani, L. Grzanka, C. Guaragnella, J. Hammerbauer, J. Heino, A. Karev, J. Kašpar, J. Kopal, V. Kundrát, S. Lami, G. Latino, R. Lauhakangas, R. Linhart, M. Lokajíček, L. Losurdo, M. L. Vetere, F. L. Rodríguez, D. Lucsanyi, M. Macrí, A. Mercadante, N. Minafra, S. M. Toli, T. Naaranoja, F. Nemes, H. Niewiadomski, T. Novak, E. Oliveri, F. Oljemark, M. Orinno, K. Österberg, P. Palazzi, L. Paločko, V. Passaro, Z. P. tka, V. Petruzzelli, T. Politi, J. Procházka, F. Prudeniano, M. Quinto, E. Radermacher, E. Radicioni, F. Ravotti, E. Robutti, C. Royon, G. Ruggerio, H. S. o, A. Scribano, J. Smajek, W. Snoeys, J. Sziklai, C. Taylor, N. Turini, V. Vacek, J. Welti, P. Wyszowski, and K. Zielinski, “Diamond detectors for the TOTEM timing upgrade,” *Journal of Instrumentation*, vol. 12, pp. P03007–P03007, mar 2017.
- [5] M. Booth, G. Forcolin, V. Grilj, B. Hamilton, I. Haughton, M. McGowan, S. Murphy, A. Oh, P. Salter, I. Sudić, and N. Skukan, “Study of cubic and hexagonal cell geometries of a 3d diamond detector with a proton micro-beam,” *Diamond and Related Materials*, vol. 77, pp. 137 – 145, 2017.
- [6] B. Caylar, M. Pomorski, and P. Bergonzo, “Laser-processed three dimensional graphitic electrodes for diamond radiation detectors,” *Applied Physics Letters*, vol. 103, p. 043504, jul 2013.
- [7] F. Bachmair, L. Bä, P. Bergonzo, B. Caylar, G. Forcolin, I. Haughton, D. Hits, H. Kagan, R. Kass, L. Li, A. Oh, S. Phan, M. Pomorski, D. S. Smith, V. Tyzhnevyyi, R. Wallny, and D. Whitehead, “A 3D diamond detector for particle tracking,” *NIM Phys A* 786, 2015.
- [8] S. Lagomarsino, M. Bellini, C. Corsi, F. Gorelli, G. Parrini, M. Santoro, and

- S. Sciortino, “Three-dimensional diamond detectors: Charge collection efficiency of graphitic electrodes,” *Applied Physics Letters* 103, 2013.
- [9] T. Kononenko, M. Meier, M. Komlenok, S. Pimenov, V. Romano, V. Pashinin, and V. Konov, “Microstructuring of diamond bulk by IR femtosecond laser pulses,” *Applied Physics A*, vol. 90, pp. 645–651, Dec. 2008.
- [10] S. Lagomarsino, M. Bellini, C. Corsi, V. Cindro, K. Kanxheri, A. Morozzi, D. Passeri, L. Servoli, C. J. Schmidt, and S. Sciortino, “Radiation hardness of three-dimensional polycrystalline diamond detectors,” *Applied Physics Letters*, vol. 106, no. 19, p. 193509, 2015.
- [11] A. Oh, B. Caylar, M. Pomorski, and T. Wengler, “A novel detector with graphitic electrodes in CVD diamond,” *Diamond and Related Materials*, 38, 2013.
- [12] G. Forcolin, *Development and Simulation of 3D Diamond Detectors*. University of Manchester, 2018.
- [13] ElementSix, *E6 CVD Diamond Handbook*, 2015 (accessed 6th October 2020).
- [14] P. S. Salter, M. Baum, I. Alexeev, M. Schmidt, and M. J. Booth, “Exploring the depth range for three-dimensional laser machining with aberration correction,” *Opt. Express*, vol. 22, pp. 17644–17656, Jul 2014.
- [15] R. D. Simmonds, P. S. Salter, A. Jesacher, and M. J. Booth, “Three dimensional laser microfabrication in diamond using a dual adaptive optics system,” *Opt. Express*, vol. 19, pp. 24122–24128, Nov 2011.
- [16] T. Kononenko, V. Ralchenko, A. Bolshakov, V. Konov, P. Allegrini, M. Pacilli, G. Conte, and E. Spiriti, “All-carbon detector with buried graphite pillars in CVD diamond,” *Applied Physics A*, vol. 114, no. 2, pp. 297–300, 2013.
- [17] B. Sun, P. S. Salter, and M. J. Booth, “High conductivity micro-wires in diamond following arbitrary paths,” *Applied Physics Letters*, vol. 105, no. 23, p. 231105, 2014.
- [18] M. Girolami, L. Criante, F. D. Fonzo, S. L. Turco, A. Mezzetti, A. Notargiacomo, M. Pea, A. Bellucci, P. Calvani, V. Valentini, and D. M. Trucchi, “Graphite distributed electrodes for diamond-based photon-enhanced thermionic emission solar cells,” *Carbon*, vol. 111, pp. 48 – 53, 2017.
- [19] K. Ashikkalieva, T. Kononenko, E. Obraztsova, E. Zavedeev, A. Khomich, E. Ashkinazi, and V. Konov, “Direct observation of graphenic nanostructures inside femtosecond-laser modified diamond,” *Carbon*, vol. 102, pp. 383 – 389, 2016.
- [20] P. S. Salter, M. J. Booth, A. Courvoisier, D. A. J. Moran, and D. A. MacLaren, “High resolution structural characterisation of laser-induced defect clusters inside diamond,” *Applied Physics Letters*, vol. 111, no. 8, p. 081103, 2017.
- [21] M. Shimizu, Y. Shimotsuma, M. Sakakura, T. Yuasa, H. Homma, Y. Minowa, K. Tanaka, K. Miura, and K. Hirao, “Periodic metallo-dielectric structure in diamond,” *Opt. Express*, vol. 17, no. 1, pp. 46–54, 2009.
- [22] C. Manfredotti, F. Wang, P. Polesello, E. Vittone, F. Fizzotti, and A. Scacco, “Blue-violet electroluminescence and photocurrent spectra from polycrystalline chemical vapor deposited diamond film,” *Applied Physics Letters*, vol. 67, no. 23, pp. 3376–3378, 1995.
- [23] J. Forneris, A. Battiato, D. G. Monticone, F. Picollo, G. Amato, L. Boarino, G. Brida, I. Degiovanni, E. Enrico, M. Genovese, et al., “Electroluminescence from a diamond device with ion-beam-micromachined buried graphitic electrodes,” *Nuclear Instruments and Methods in Physics Research Section B: Beam Interactions with Materials and Atoms*, vol. 348, pp. 187–190, 2015.
- [24] I. Lopez Paz, O. Allegre, Z. Li, A. Oh, A. Porter, and D. Whitehead, “Study of



electrode fabrication in diamond with a femto-second laser,” *Phys. Status Solidi A*, vol. 216, no. 21, p. 1900236, 2019.

- [25] T. Wulz, B. K. Canfield, L. M. Davis, S. Spanier, and E. Lukosi, “Pulsed femtosecond-laser machining and deep reactive ion etching of diamond,” *Diamond and Related Materials*, vol. 74, pp. 108 – 113, 2017.
- [26] S. Kumar, B. Sotillo, A. Chiappini, R. Ramponi, P. Di Trapani, S. M. Eaton, and O. Jedrkiewicz, “Study of graphitic microstructure formation in diamond bulk by pulsed bessel beam laser writing,” *Applied Physics A*, vol. 123, p. 698, Oct 2017.
- [27] C. Bloomer, M. E. Newton, G. Rehm, and P. S. Salter, “A single-crystal diamond X-ray pixel detector with embedded graphitic electrodes,” *Journal of Synchrotron Radiation*, vol. 27, pp. 599–607, May 2020.
- [28] C. J. Stephen, B. L. Green, Y. N. D. Lekhai, L. Weng, P. Hill, S. Johnson, A. C. Frangeskou, P. L. Diggle, Y.-C. Chen, M. J. Strain, E. Gu, M. E. Newton, J. M. Smith, P. S. Salter, and G. W. Morley, “Deep three-dimensional solid-state qubit arrays with long-lived spin coherence,” *Phys. Rev. Applied*, vol. 12, p. 064005, Dec 2019.